

# Realistic transport modeling for a superconducting nanowire with Majorana fermions

Diego Rainis, Luka Trifunovic, Jelena Klinovaja, and Daniel Loss

Department of Physics, University of Basel, Klingelbergstrasse 82, CH-4056 Basel, Switzerland

(Dated: April 5, 2022)

Motivated by recent experiments searching for Majorana fermions (MFs) in hybrid semiconducting-superconducting nanostructures and by subsequent theoretical interpretations, we consider the so far most realistic model (including disorder) and analyze its transport behavior numerically. In particular, we include in the model superconducting contacts used in the experiments to extract the current. We show that important new features emerge that are absent in simpler models, such as the enhanced visibility of the topological gap for increased spin-orbit interaction. We find oscillations of the zero bias peak as function of magnetic field and explain their origin. Even taking into account all the possible (known) ingredients of the experiments and exploring many parameter regimes for MFs, we are not able to reach a satisfactory agreement with the reported data. Thus, a different physical origin for the observed zero-bias peak cannot be excluded.

PACS numbers: 74.45.+c, 73.63.Nm, 74.78.Na

The experimental search [1–3] of Majorana fermions (MFs) predicted to occur in condensed matter systems [4–10] is very challenging due to the fact that these exotic quasiparticles are characterized by zero effective coupling to electromagnetic fields. Only an indirect identification is possible via induced signatures. For instance, the presence of a MF is expected to induce a zero-bias conductance peak (ZBP) in a tunnel-spectroscopy transport experiment [11, 12]. However, such features while being easily observable, are not an unambiguous demonstration of MF physics. The same ZBPs can indeed be induced by various different mechanisms, including the Kondo effect [13], Andreev bound states [14], weak antilocalization and reflectionless tunneling [15]. Ruling out these alternative scenarios has been made difficult by the fact that the measured conductance has a rather unexpected behavior, so that also the explanation in terms of MFs is not entirely satisfactory.

A typical experimental setup [1–3] (see Fig. 1) consists of a spin-orbit-coupled semiconducting nanowire deposited on or coated with a bulk *s*-wave superconductor on one end and contacted through a tunnel barrier by a normal lead, on the other end. Part of the nanowire itself is assumed to be in a superconducting state, induced through proximity effect by the bulk superconducting lead.

The magnetic-field-induced transition to the topological phase in the nanowire is accompanied by a closing and reopening of the excitation gap [5–10]. The topological phase formally persists for all values of magnetic field above a critical  $B_c$  in a one-band model, while it could have a finite upper critical field in a multi-band model, where bands are crossing at large Zeeman splittings and hybridization of MFs can take place. However, in experiments one typically explores magnetic field regimes where only one band undergoes a topological transition [1–3]. Since the bulk superconductor always remains in a non-topological state, the topological sec-

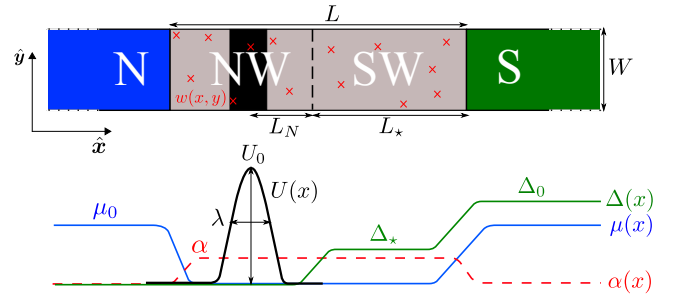


FIG. 1. The schematics of the NSS' geometry setup we consider in this work— (top panel). The sample under investigation is connected on the left to a semi-infinite normal lead (N, orange) and on the right to a semi-infinite bulk *s*-wave superconducting lead (S, green). It consists of a normal nanowire section (NW, gray), where a potential barrier  $U(x)$  (black) is created, and a proximity-induced superconducting nanowire section (SW, gray). We allow for static disorder  $w(x, y)$  (red crosses) in the nanowire. The spatial dependence of all the parameters entering the Hamiltonian in Eq. (1) is qualitatively depicted in the bottom panel.

tion has a finite length  $L_*$ , and MFs localized at its ends can overlap, depending on their localization length  $\xi_M$ . Given that the latter depends also on the value of magnetic field, one expects to observe a ZBP that splits for large enough  $B$ -fields.

The experiments conducted so far [1–3] reported features which are *partially* consistent with the existence of Majorana end-states in the nanowire, namely a (non-quantized) ZBP when a magnetic field of sufficient strength is applied along the nanowire. However, *quantitative* agreement with the theory is still missing, and in particular the following points have to be clarified:

a) The most evident discrepancy between experiment and theory is the absence of any experimental signature related to the closing of the excitation gap in the nanowire. Recently, this fact has been ascribed to the

spatial distribution of the wave-functions associated with the closing-gap-states in the regime of low chemical potential [16, 17].

b) The ZBP in the experiments appears above a certain magnetic field, persists over a finite range of values, and then disappears again symmetrically, rather than mutating into a pair of split peaks as expected for MFs.

c) The ZBP conductance is not quantized, with values being a small fraction of the quantum of conductance  $2e^2/h$  [1–3], while in theory the Majorana is providing a full transport channel and produces a quantized conductance peak  $G = 2e^2/h$  [11, 18, 19].

d) The proximity-induced gap  $\Delta_*$  in the nanowire depends only very weakly on magnetic field in the measured  $dI/dV$  curves, and the corresponding conductance signal decreases significantly above a certain magnetic field [1, 3]. Such sudden reduction is not predicted by the theory, and the gap should close much faster as a function of magnetic field. This issue has not been pointed out in previous theoretical studies.

In an attempt to find explanations for above issues, we have performed numerical calculations of the two-terminal conductance in an hybrid structure with a superconducting spin-orbit-coupled nanowire contacted on one side by a normal metallic lead and on the other side by a standard  $s$ -wave superconducting lead, referred to as NSS' setup (see Fig. 1), which closely resembles the actual geometry of the experiment. The conductance is calculated within the standard framework of scattering theory [20], with the help of the recursive Green's function technique [21] applied to a real-space tight-binding Hamiltonian. Such a procedure allows us to model a complex structure like the one effectively involved in an experimental situation that is not amenable to analytical approaches [22].

To be specific, we focus now on energy scales appropriate for InSb nanowires [1, 2], with the exceptions and specifications described below. Nonidealities and complications such as multiple occupied sub-bands, presence of disorder, finite width of electrostatic barriers, finite coherence lengths of superconducting pairing amplitudes, and non-zero temperature are taken into account.

Our study reveals important features not emphasized so far. In this respect, the presence of the bulk superconductor turns out to be decisive. We briefly summarize here our main findings. In some regimes, the closing of the gap becomes visible in the conductance signal, while it does not in an NS-setup simulation. Further, the gap-edge conductance peak value decreases as a function of magnetic field, a feature which is also not captured by simpler models. We find oscillations of the zero bias peak as function of  $B$  and explain their origin. We argue that disorder is unlikely to be the explanation for the ZBPs observed in experiments. Further, we show that the tunnel barrier plays an important role in determining which features are actually visible. Finally, according to our

results the experimental  $dI/dV$  behavior seems to point to a SOI strength larger than the one reported.

*Model.* We consider a two-dimensional rectangular nanowire of length  $L$  along the  $\hat{x}$ -direction and lateral extension  $W$  in the  $\hat{y}$ -direction. The general tight-binding Hamiltonian describing the different sections of the setup in the presence of a magnetic field has the form

$$H = \sum_{\mathbf{m}, \mathbf{d}} c_{\mathbf{m}+\mathbf{d}, \alpha}^\dagger \left[ -t\delta_{\alpha\beta} - i\alpha_{\mathbf{m}}(\hat{\mathbf{x}} \cdot \mathbf{d})\sigma_{\alpha\beta}^y \right] c_{\mathbf{m}, \beta} + \sum_{\mathbf{m}} c_{\mathbf{m}, \alpha}^\dagger \left[ (\epsilon_{\mathbf{m}} - \mu_0)\delta_{\alpha\beta} - \frac{g_{\mathbf{m}}}{2}\mu_B B_x \sigma_{\alpha\beta}^x \right] c_{\mathbf{m}, \beta} + \sum_{\mathbf{m}} \Delta_{\mathbf{m}} \left( c_{\mathbf{m}, \uparrow}^\dagger c_{\mathbf{m}, \downarrow}^\dagger + \text{h.c.} \right), \quad (1)$$

where  $t$  is the hopping amplitude and  $\alpha$  is the spin-flip hopping amplitude, related to the spin-orbit interaction (SOI) energy  $E_{\text{so}}$  through the relation  $E_{\text{so}} = \alpha^2/t$ . The sum in the first row runs over all lattice sites  $\mathbf{m}$  and relative nearest neighbors  $(\mathbf{m} + \mathbf{d})$ . Implicit summation over repeated spin indices is assumed. The constant  $\mu_0$  is chosen to set the common chemical potential to the zero-field bottom of the topmost band in the nanowire, and its value depends on the number of nanowire sub-bands (i.e. on  $W$ ). The term  $\epsilon_{\mathbf{m}} = -\mu_{\mathbf{m}} + U_{\mathbf{m}} + w_{\mathbf{m}}$  accounts for local variations of the chemical potential, for the tunnel-barrier potential  $U_{\mathbf{m}}$ , and includes an on-site random potential  $w_{\mathbf{m}}$  which models Anderson disorder. The tunnel barrier is assumed to have a Gaussian profile with height  $U_0$  and width  $\lambda$ . An external magnetic field  $\mathbf{B}$  is oriented along the nanowire axis ( $\hat{x}$ ) and induces a Zeeman splitting  $2V_Z = g_{\mathbf{m}}\mu_B B$ . Finally,  $\Delta$  is the pairing amplitude and can either account for the native superconductivity in the bulk  $s$ -wave superconducting lead ( $\Delta_0$ ) or for the proximity-induced pairing in the nanowire ( $\Delta_*$ ). All these quantities are taken to be site-dependent along the  $\hat{x}$  direction (except  $w_{\mathbf{m}}$ , which is taken to be completely random), so that by varying their value we can model physically different parts of the setup. The normal lead is characterized by  $\alpha = 0$ ,  $\mu \simeq \mu_0$  (i.e. metallic regime),  $g = 2$ ,  $w_{\mathbf{m}} = 0$ , and  $\Delta = 0$ . The nanowire is characterized by finite  $\alpha = \alpha_R$ , chemical potential  $\mu \simeq 0$  close to the bottom of the top-most band,  $g = 50$  appropriate for InSb nanowires, and  $\Delta$  varying from 0 in the normal section to  $\Delta_*$  in the proximized section. The nanowire is adiabatically connected to a metallic superconducting lead with  $\alpha = 0$ ,  $\mu \simeq \mu_0$ ,  $g = 2$ ,  $w_{\mathbf{m}} = 0$ , and  $\Delta = \Delta_0 \geq \Delta_*$ . By adopting the sequential geometry of Fig. 1, we slightly simplify here the actual situation in the experiments [1–3], where the nanowire is side-contacted, or top-contacted, and the current does not follow a straight path.

In a simpler model the nanowire can be taken to extend to infinity, without any external superconductor, in an effective NS geometry. In our formalism this corresponds to taking the superconducting lead to be

physically identical to the nanowire, with a single pairing amplitude  $\Delta_*$ . In such a configuration, the second Majorana end-state is always moved to infinity, and the ZBP is locked to zero for all values of magnetic field  $B > B_c$ , whereby the topological transition occurs at the critical field  $(g\mu_B/2)B_c = \sqrt{\Delta_*^2 + \mu^2}$  [5–10]. We will sometimes switch to this NS configuration in order to make contact to previous theoretical studies [16, 17, 23–27] and to understand the effect of the bulk superconductor.

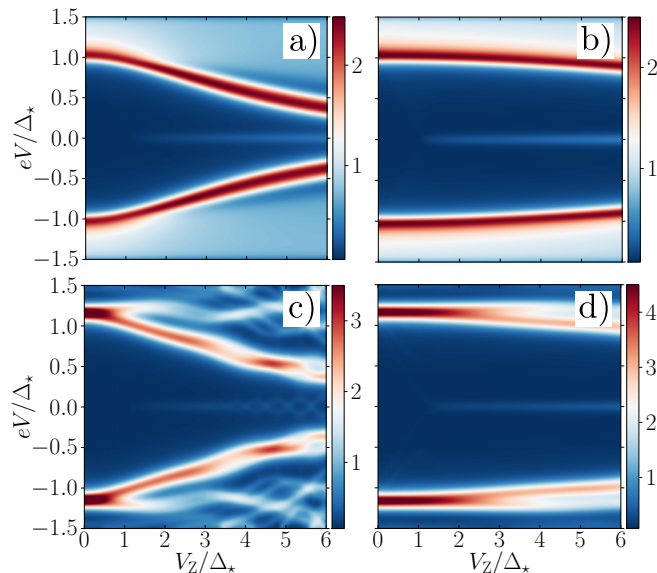


FIG. 2. Effect of larger SOI strength. We plot here the differential conductance  $dI/dV$  evaluated as a function of bias voltage  $V$  and Zeeman energy  $V_Z$ . Panels a) and b) refer to the NS configuration, while c) and d) refer to the NSS' setup. The parameters used here are  $\Delta_* = 250 \mu\text{eV}$ ,  $\Delta_0 = 2.1 \text{ meV}$  (only NSS'),  $U_0 = 45 \text{ meV}$ ,  $\lambda = 1 \text{ nm}$  (narrow barrier),  $L_N = 0$ ,  $L_* = 6 \mu\text{m}$  (only NSS') and  $\mu = 0$ , which corresponds to a critical  $V_Z^c = \Delta_*$ . For the case of InSb, the plotted range  $V_Z = 0 - 6\Delta_*$  corresponds to  $B = 0 - 1 \text{ T}$ . Temperature is set to  $T = 75 \text{ mK}$ . (Left column)  $E_{\text{so}} = 50 \mu\text{eV}$ . (Right column)  $E_{\text{so}} = 200 \mu\text{eV}$ . Larger SOI yields a slower closing of the  $k_F$ -gap  $\Delta_{k_F}(B)$ , in both configurations, where  $k_F$  is the Fermi momentum. Notice that in the NSS' case the  $k_F$ -gap signal decreases in intensity as the magnetic field grows.

Let us first note that the actual value of the SOI  $\alpha$  in the experiments is not known, as also noticed in Ref. [28], since the only available measurements have been performed in a different setup, where the effective Rashba SOI could be largely modified. Similarly, the value of the proximity-induced pairing amplitude is not directly accessible, and one can only infer its value from the conductance peaks. Having said that, it becomes interesting and even necessary to consider regimes with different SOI, or different proximity-induced gap magnitudes.

The first important point we want to make is that by assuming that the actual SOI is larger than the reported one (e.g.  $E_{\text{so}} = 50 \mu\text{eV}$  in Ref. [1]), one can get a sub-

stantial improvement in the calculated  $dI/dV$  behavior, with features resembling closer the ones observed in experiments [1–3]. In other words, the data gives hints of a stronger SOI. In particular, we note the following facts.

1) Under the assumption that the ZBP observed in Refs. [1–3] arises from MFs, one must conclude that the chemical potential in the topological region is low,  $\mu \simeq 0$ , since the ZBP emerges at low magnetic field,  $\frac{1}{2}g\mu_B B \simeq \Delta_*$  for  $g = 50$ , which implies a low  $\mu$  in view of the relation between  $B_c$ ,  $\mu$ , and  $\Delta_*$ . However, such a low  $\mu$ , together with the reported SOI values [1], would generate a rapid closing of the  $k_F$ -gap  $\Delta_{k_F}$  as a function of magnetic field. This is indeed what we observe in our numerical calculations when we work in the regime  $\mu \simeq 0$ ,  $E_{\text{so}} = 50 \mu\text{eV}$ , both in the NS and NSS' setup, see Fig. 2a) and c), respectively. Note that in the NS case the ZBP stays at zero bias for all magnetic fields, whereas in the NSS' case the finite length of the topological region induces an oscillating splitting, analyzed below. In the same figure we show that a stronger SOI gives better agreement with the measured  $\Delta_{k_F}(B)$ , both in the NS setup [24], see panel b), and in the NSS' setup, shown in panel d). Note that this latter SOI effect is independent of the nature of the observed ZBP.

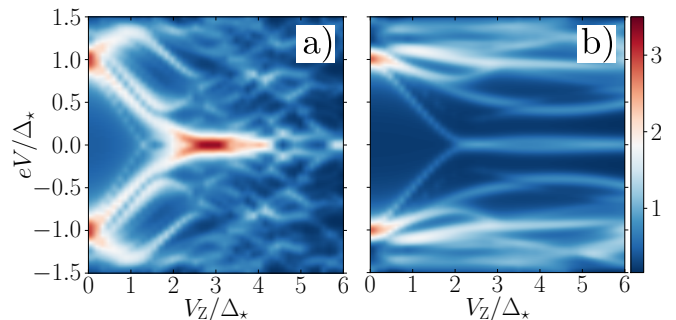


FIG. 3. Effect of larger SOI strength on disorder, NSS' case. The parameter values are the same as in Fig. 2. In addition, a realistic disorder  $w_m \in [-2.4, 2.4] \text{ meV}$  (corresponding to a mean free-path  $\ell_{\text{mfp}} \simeq 2.5 \mu\text{m}$  [28]) is included over the entire nanowire length  $L \simeq 2.5 \mu\text{m}$ . We do not average over disorder configurations. a)  $E_{\text{so}} = 50 \mu\text{eV}$ . b)  $E_{\text{so}} = 200 \mu\text{eV}$ . In the weak SOI regime, the disorder lowers or destroys the gap from other sub-bands, bringing many supra-gap states down close to the Fermi level, where they cluster in some cases into a finite-extension ZBP, like in panel a). Such clustering is, however, removed for stronger SOI [28], see panel b).

2) When realistic Anderson disorder is included in the model, the closing of the gap becomes visible again even in the  $\mu \simeq 0$  regime [17, 26, 28], re-introducing a discrepancy with the experimental observations [1–3]. Disorder in a *weakly* spin-orbit-coupled nanowire causes a number of sub-gap states to appear, some of which cluster around zero-energy and possibly give rise to a non-topological ZBP, more markedly in the case of finite  $\mu$  [28]. Such states are coming from other sub-bands, for which the

effective mini-gap gets reduced in the presence of disorder. This is substantiated by the fact that the ZBP in Fig. 3a) has a conductance peak value larger than  $2e^2/h$ , implying that it cannot come from the Andreev signal of a single state. In the case of stronger SOI, the effect of disorder is partially suppressed, and less sub-gap states (or no states at all) are observed (see Fig. 3), being more compatible with experiments [1–3]. Thus, disorder is unlikely to explain the observed ZBPs.

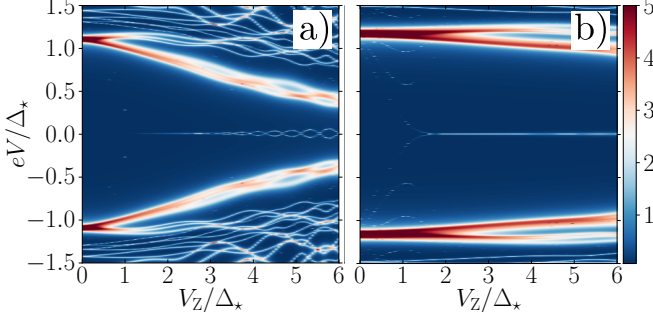


FIG. 4. Same parameters as in previous figures, without disorder and at  $T = 0$ . (a)  $E_{\text{so}} = 50 \mu\text{eV}$ . Note the oscillations of the ZBP, for explanations see text. (b)  $E_{\text{so}} = 200 \mu\text{eV}$ . With large enough SOI strength the gap-closing becomes visible, even for the considered case of  $\mu \simeq 0$ , while it is not visible in an NS setup with the same parameters. The  $dI/dV$  peaks coming from the gap-closing have, however, very small width and they get washed out by realistic temperatures.

3) As a consequence of finite-length of the topological section ( $L_*$ ) and of the  $B$ -dependence of  $k_F$ , we observe that the ZBP splitting exhibits oscillations as  $B$  is swept, see Fig. 4a). To explain this, we recall that in the weak-SOI limit the MF wave function has an exponentially decaying envelope with localization length  $\xi_M$  and a fast-oscillating part  $\sim \sin(k_F x)$  [29]. If the magnetic field exceeds a critical value  $B_c^*$  (see Fig. 5), the two end-MFs overlap and split away from zero energy. Since  $\xi_M$  increases with  $B$  [5–10, 29], so does the splitting. However, if  $k_F L_*$  becomes an integer multiple of  $\pi$  as function of  $B$ , the ZBP splitting returns to zero, leading to oscillations with period given by

$$\delta(V_Z/\Delta_*) = \frac{\pi\hbar}{L_*\Delta_*} \sqrt{\frac{2V_Z}{m}} = \frac{\pi a}{L_*} \frac{\sqrt{tV_Z}}{\Delta_*}, \quad (2)$$

where  $m$  is the band mass and  $a$  the lattice constant. Using parameter values corresponding to Fig. 4,  $t/\Delta_* = 40$ ,  $L_*/a = 200$ , we obtain quantitative agreement with the simulated ZBP oscillations. Since the critical field  $B_c^*$  increases with SOI [29], the ZBP splitting and related oscillations occur at larger fields, see Fig. 4b). Note that these oscillations are quite robust against temperature effects, see Fig. 2c). This behavior of the ZBP is quite remarkable and provides an additional signature to identify MFs experimentally.

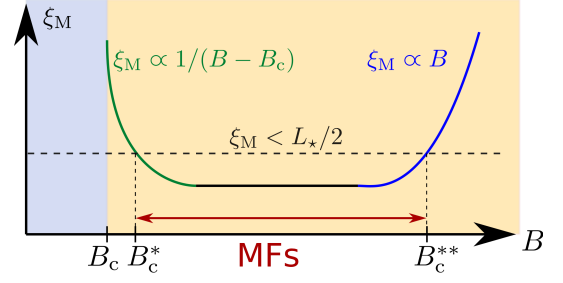


FIG. 5. Schematic dependence of the MF localization length  $\xi_M$  on magnetic field  $B$ . According to the theory for a one-band semi-infinite nanowire [9, 10], a MF emerges when the magnetic field exceeds a critical value  $B_c = 2\sqrt{\Delta_*^2 + \mu^2}/g\mu_B$ , and the system goes from the non-topological (grey) to the topological (yellow) regime. However, for a nanowire of finite length  $L_*$ , due to overlap of the MFs from each end, the additional condition for the observation of a MF is  $\xi_M < L_*/2$ . Considering typical dependences of  $\xi_M$  on magnetic field [29], we predict that the MF should be observed for  $B_c^* < B < B_c^{**}$ , where  $\xi_M(B_c^*) \approx \xi_M(B_c^{**}) \approx L_*/2$  (cf. Fig. 4).

We note in passing that in the NSS' setup the SOI affects the visibility of the gap-closing, see Fig. 4. This is not the case for the NS setup.

Next we address further issues that have received less attention in the literature so far.

4) The position of the proximity gap  $\Delta_{k_F}(B = 0)$  deduced from the  $dI/dV$  curves is in general different from the nominal value  $\Delta_*$  inserted in the microscopic Hamiltonian, Eq. (1). This observation is important, since it could mean that deducing the value of the proximity-induced gap from the conductance spectra is not a correct procedure [1, 3]. Such an energy shift can be due to the presence of a finite normal region between the tunnel barrier and the effective NS interface. In that case, the observed peak occurs at a bias voltage *lower* than the

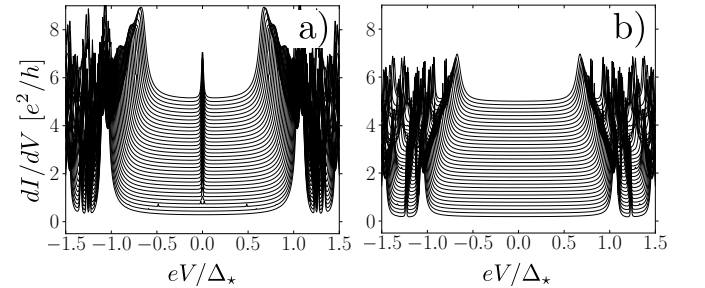


FIG. 6. Role of the tunnel barrier  $U(x)$ . The parameters are chosen as in the previous figures. Here we kept  $T = 0$  in order to show the effect of the barrier smoothness alone. a) Gaussian tunnel barrier with width  $\lambda = 1 \text{ nm}$ . The Majorana-induced ZBP is fully visible, with maximal weight  $dI/dV = 2e^2/h$  at the largest magnetic fields. The closing of the gap is, however, nearly absent. b) Same system, but with  $\lambda = 50 \text{ nm}$ , a value closer to the experimental situation. Gap-closing and ZBP are completely absent.

nominal  $\Delta_*$ . By increasing the distance of the barrier from the NS interface, one can move the conductance peak deeper inside the gap and eventually even introduce additional peaks, similar to the McMillan-Rowell resonances [30]. Alternatively, in the NSS' configuration the peak corresponding to  $\Delta_*$  itself can be viewed as a sub-gap resonance of the larger gap  $\Delta_0$ , and its position can be changed by varying the distance of the tunnel barrier from the S-S' interface. In this case, the peak has energy *larger* than the microscopic value of  $\Delta_*$ .

5) In both NS and NSS' configurations, the tunnel barrier plays an important role—it determines the transmission of each transport channel, which in turn sets the width of the McMillan-Rowell resonances [30]. When the resonance width becomes smaller than the temperature, the resonance is practically invisible. Consequently, if the barrier is wide enough, no sub-gap features at all are present in the  $dI/dV$  signal. This can be attributed to the associated maximum momentum mismatch  $\sim \lambda^{-1}$  that the barrier can provide to an incoming electron. If the tunnel barrier is chosen to be sharp, all the states present in the nanowire could in principle be made visible. However, that is not a realistic choice, since a typical barrier in experiments has a characteristic width of  $\sim 50$  nm. For such values we already observe a momentum filtering due to the barrier, leading in some cases to a complete disappearance of MF signatures, see Fig. 6. Again, introducing disorder can make the aforementioned sub-gap features re-appear. Therefore, it is the combined effect of barrier shape, SOI, and disorder strength that determines the visibility of MFs.

In conclusion, by numerically simulating a more complex and realistic setup than before, we have obtained new features in the transport simulations, which are similar to the ones observed in experiments. However, even after considerable effort, we did not manage to reproduce all such features in a single configuration, and we still lack a satisfactory agreement with experiments. In particular, the exact shape of the measured ZBP is not very compatible with the picture of MF states that form and then split as a function of magnetic field. Thus, a different physical origin for the observed ZBP [1–3] cannot be excluded. More precisely, from our findings it seems possible that in the experiments the MF-features are essentially invisible and the observed ZBP is coming from some different co-existing phenomenon, like Kondo effect, which seems indeed to yield a similar behavior [31].

We thank Fabio Pedrocchi for useful discussions and Fabio Taddei for support with the numerics. This

work has been supported by the Swiss NSF, NCCR Nanoscience, NCCR QSIT, and the EU project SOLID.

- 
- [1] V. Mourik *et al.*, Science **336**, 1003 (2012).
  - [2] M. T. Deng *et al.*, arXiv:1204.4130 (2012).
  - [3] A. Das *et al.*, arXiv:1205.7073 (2012).
  - [4] S. Fujimoto, Phys. Rev. B **77**, 220501 (2008).
  - [5] M. Sato, Y. Takahashi, and S. Fujimoto, Phys. Rev. Lett. **103**, 020401 (2009).
  - [6] J. D. Sau *et al.*, Phys. Rev. Lett. **104**, 040502 (2010).
  - [7] M. Sato, Y. Takahashi, and S. Fujimoto, Phys. Rev. B **82**, 134521 (2010).
  - [8] J. Alicea, Phys. Rev. B **81**, 125318 (2010).
  - [9] R. M. Lutchyn, J. D. Sau, and S. Das Sarma, Phys. Rev. Lett. **105**, 077001 (2010).
  - [10] Y. Oreg, G. Refael, and F. von Oppen, Phys. Rev. Lett. **105**, 177002 (2010).
  - [11] K. Sengupta *et al.*, Phys. Rev. B **63**, 144531 (2001).
  - [12] J. Sau *et al.*, Phys. Rev. B **82**, 214509 (2010).
  - [13] S. Sasaki *et al.*, Nature **405**, 764 (2000).
  - [14] M. Zareyan, W. Belzig, and Y. V. Nazarov, Phys. Rev. B **65**, 184505 (2002).
  - [15] B. J. van Wees *et al.*, Phys. Rev. Lett. **69**, 510 (1992).
  - [16] T. D. Stanescu *et al.*, arXiv:1206.0013 (2012).
  - [17] F. Pientka *et al.*, arXiv:1206.0723 (2012).
  - [18] K. Law, P. A. Lee, and T. Ng, Phys. Rev. Lett. **103**, 237001 (2009).
  - [19] A. Akhmerov *et al.*, Phys. Rev. Lett. **106**, 057001 (2011).
  - [20] C. Lambert, J. Phys.: Condens. Matter **3**, 6579 (1991); C. Lambert and R. Raimondi, *ibid.* **10**, 901 (1998).
  - [21] A. MacKinnon, Z. Phys. B **59**, 385 (1985).
  - [22] Note that the SW region is not grounded in typical experiments. This can be accounted for through a modified formula for the conductance, and leads to small corrections [20, 32].
  - [23] D. Chevallier, D. Sticlet, P. Simon, and C. Bena, Phys. Rev. B **85**, 235307 (2012).
  - [24] E. Prada, P. San-Jose, and R. Aguado, arXiv:1203.4488 (2012).
  - [25] C.-H. Lin, J. Sau, and S. Das Sarma, arXiv:1204.3085 (2012).
  - [26] D. Bagrets and A. Altland, arXiv:1206.0434 (2012).
  - [27] D. I. Pikulin *et al.*, arXiv:1206.6687 (2012).
  - [28] J. Liu *et al.*, arXiv:1206.1276 (2012).
  - [29] J. Klinovaja and D. Loss, arXiv:1205.7054 (2012).
  - [30] J. M. Rowell and W. L. McMillan, Phys. Rev. Lett. **16**, 453 (1966); J. M. Rowell, *ibid.* **30**, 167 (1973); R. A. Riedel and P. F. Bagwell, Phys. Rev. B **48**, 15198 (1993).
  - [31] E. J. H. Lee *et al.*, arXiv:1207.1259 (2012).
  - [32] M. Antram and S. Datta, Phys. Rev. B **53**, 16390 (1996).